www.elsevier.com/locate/jmbbm

AFM-Based Study of Fullerenol $C_{60}(OH)_{24}$ Induced Changes of Elasticity in Living SMCC-7721 Cells

Yang Liu, Zuobin Wang, Xinyue Wang

PII: S1751-6161(14)00390-7
DOI: http://dx.doi.org/10.1016/j.jmbbm.2014.12.011
Reference: JMBBM1343

To appear in: *Journal of the Mechanical Behavior of Biomedical Materials*

Received date: 6 August 2014
Revised date: 8 December 2014
Accepted date:
10 December 2014

Cite this article as: Yang Liu, Zuobin Wang, Xinyue Wang, AFM-Based Study of Fullerenol $C_{60}(OH)_{24}$ Induced Changes of Elasticity in Living SMCC-7721 Cells, *Journal of the Mechanical Behavior of Biomedical Materials*, http://dx.doi.org/10.1016/j.jmbbm.2014.12.011

AFM-Based Study of Fullerenol $C_{60}(OH)_{24}$ Induced Changes of Elasticity in Living SMCC-7721 Cells

Yang Liu, Zuobin Wang, Xinyue Wang

CNM & JR3CN Centres

Changchun University of Science and Technology

Changchun, China

Address all correspondence to: Zuobin Wang, Changchun University of Science and Technology, CNM & JR3CN, Changchun, China, 130022; Tel: +86 43185582341, Fax: +86 43185582925; E-mail: wangz@cust.edu.cn

Abstract

In this study, the alterations of morphology and biomechanical properties of living SMCC-7721 cancer cells treated by fullerenol ($C_{60}(OH)_{24}$) for 24 h, 48 h and 72 h are investigated by atomic force microscope (AFM). Comparative analyses show that the elastic moduli of the SMCC-7721 cells exposed to the fullerenol decrease significantly with the increase of the treatment periods. Furthermore, in different phases of the treatment, a global decrease in elasticity is accompanied by cellular morphological changes, and the time-dependent effect of the fullerenol can be observed using AFM and optical microscope. In addition, as the treatment duration increases, the indentation force and depth penetrated into the cell membrane by the AFM tip are in a declining trend. The reduction in the stiffness of the cells exposed to the fullerenol could be associated with the disruption of the cellular cytoskeleton network. The investigation indicates that the elastic modulus of single living cells can be a useful biomarker to evaluate the effects of the fullerenol or other anticancer agents on the cells and reveal instructive information for cellular dynamic behaviors.

***Keywords*:** Atomic force microscope (AFM); SMCC-7721 cell; Morphology; Elastic modulus; Fullerenol; Nanoindentation

1. Introduction

The fullerene family possesses unique physical and chemical properties for potential applications in biomedicine such as cancer diagnosis and therapy (Chen et al., 2010; Chen et al., 2012; Partha et al., 2009). The native fullerenes (C_{60}) with the lack of solubility result in aggregation in aqueous solutions and have high toxicity (Chen et al., 2010; Nielsen et al., 2008; Partha et al., 2009; Shimizu et al., 2013; Sayes et al., 2004), which hinders their applications in biomedicine, while water-soluble fullerenes, as a class of fullerene derivatives, can be synthesized by the addition of hydroxyl groups onto fullerene molecules and are termed as fullerenol ($C_{60}(OH)_n$). Consequently, some of them improve the solubility of fullerenes and increase their use in biomedicine or pharmaceutic applications (Jensen et al., 1996; Rade et al., 2008). Recently, some studies have been reported that the effects of carbon-based nanomaterials on the cytoskeletal structure (Tian et al., 2006; Walker et al., 2009; Dong et al., 2013) and the dynamical changes in cytoskeleton will affect the cell behaviors, including the migration, differentiation, and apoptosis or shape maintaining. Researchers have proposed a number of models to study and describe the apoptosis process. In different apoptosis stages, the cell shrinkage, swelling and rounding can be observed in many types of cells (Imajoh et al., 2004; Desjardins and MacManus, 1995; Saraste and Pulkki, 2000). And an increasing number of evidences shows that the disruption of the actin cytoskeleton may be an initiating apoptotic event. Among the literatures, Zhou et al. (2006) have suggested that the disruption of the actin cytoskeleton can induce apoptosis. Moreover, Johnson-Lyles et al. (2010) exposed the renal proximal tubule cells to fullerenol and have found that the fullerenol cytotoxicity induced apoptosis is associated with the cytoskeleton disruption. In addition, the anti-proliferative effect and specific photophysical properties of the fullerenol make it a potential antitumor or anticancer agent (Foleya et al., 2001; Lu et al., 1998). More importantly, the identification of cancer cells affected by fullerenols could enhance the

understanding of the role and influence of fullerenols, and reveal the potential of the cancer progression amelioration by combining nanoscience and biomechanics.

It is demonstrated that nanobiomechanics is distinctly useful to study cancer development, human disease and mechanisms of drug actions (Lee et al., 2007; Maciaszek and Lykotrafitis, 2011; Rotsch et al., 1997). The investigation of the changes of elastic stiffness in the cancer progression is helpful to understand the individual differences between normal cells and cancer cells (Plodinec et al., 2012). A number of studies shows that fullerenols can inhibit cancer cells or tumor proliferation and induce apoptosis in exposed cells (Bosi et al., 2003; Chen et al., 2012; Lu et al., 1998). They could inhibit the synthesis of microtubules and disrupt actin filaments (Johnson-Lyles et al., 2010; Mrdanović et al., 2009). Both of them not only serve as structural elements in the cytoskeleton of the cells (Etienne-Manneville, 2004; Fuchs et al., 2001) but also are able to regulate the mechanical stability of living cells (Unterberger et al., 2013). The alterations of cellular elastic stiffness directly reflect the changes of the cytoskeletons and affect the cellular processes (Aryaei and Jayasuriya, 2013; Mason et al., 2012; Nikolaev et al., 2014). The experimental study of cellular elastic stiffness on micro and nano scales could provide instructive information for the cancer progression. The mechanical measurement of individual living cells by means of the atomic force microscope (AFM) indentation is accurate (Yoo et al., 2014; Zhu et al., 2011). Since the AFM was invented in 1986 (Binnig et al., 1986), it has been rapidly developed into a powerful tool for nanoscale characterization and modification because of the high sensitivity for the detection of cantilever deformation and realized high precision controllability on the nanoscale. Moreover, it provides a promising way for the study of living cells in vitro, as 3D imaging and real-time force measurements of biological cells can be achieved by AFM in physiological environments. For instance, it can be seen, from the indentation force-displacement curves of the cantilever

deformation versus the displacement of the piezo scanner, that the elastic moduli of some cancer cells are significantly different from normal cells (Fuhrmann et al., 2011; Lekka et al., 1999; Plodinec et al., 2012). Thus, the elastic modulus of single living cells can be regarded as a biomarker for the metastasis or spread potential of some cancer cells or tumor cells (Cross et al., 2007; Jonietz, 2012; Kumar and Weaver, 2009; Lautenschläger et al., 2009; Li et al., 2008; Xu et al., 2012) and for drug efficacy testing.

Although some efforts have been made to study living cancer cells by AFM in recent years, there is still lack of knowledge or evidence that clearly confirms the relationships between biomechanical properties of living cells and their dynamic cellular processes, and there is also no reference that shows the effects of fullerenol ($C_{60}(OH)_{24}$) on the biomechanical properties of living cancer cells. According to the WHO investigation in 2012, the liver cancer is the second common cause of cancer deaths (0.8 million, 9.1%) (http://globocan.iarc.fr/Default.aspx). In this work, the human hepatocellular carcinoma (SMCC-7721) was selected as the research object. An AFM was employed to examine the changes of elastic moduli on the SMCC-7721 cells and the cells treated by fullerenol ($C_{60}(OH)_{24}$) for 24 h,48 h and 72 h, respectively. The morphological and biomechanical cellular changes caused by fullerenol were investigated using the AFM topography and nanoindentation. The investigation suggests that the measurements of the biomechanical properties of single living SMCC-7721 cells treated by fullerenol could be used to evaluate the effect of fullerenol or other anticancer agents on the cells and can represent a crucial part of the potential cancer progression.

2. Materials and methods

2.1 Cell culture

Human hepatocellular carcinoma (SMCC-7721) cells were grown in the RPMI-1640 media with 10% of Foetal Bovine Serum (FBS) and antibiotics (Penicillin-Streptomycin Solution). The cells were maintained in a humidified incubator with 5% of CO_2 at the temperature of 37 ºC. Flasks containing cells were treated with trypsin. The cells were dispersed and plated on glass coverslips (18×18 mm) at a density of 1.0×10^5 cells/mL (1 mL per coverslip) in 38 mm plastic Petri culture dishes and incubated for 24 h at 37 ºC.

2.2 Preparation of fullerenol treatment solution

The commercial water-soluble fullerenol powder with the general formula $C_{60}(OH)_{24}$ was dissolved in the deionized water at the concentration of 2.7 μM/mL and then diluted with RPMI-1640 media with 10% of FBS to 0.53 μM/mL which was used for the fullerenol treatment solution stored at 4ºC.

2.3 Sample preparation

SMCC-7721 cells were dispersed and plated on glass coverslips. After 24 h, they were washed with phosphate saline buffer (PBS) to remove unbound and dead cells, and then continuously incubated with the fullerenol treatment solution at 37ºC in a humidified incubator with 5% of CO_2 for 24 h, 48 h and 72 h, respectively. A 2-ml fullerenol treatment solution was added to each of plastic Petri culture dishes. After incubation, the exposed cells were washed with PBS and measured by AFM in the RPMI-1640 media. The control cells, unexposed to the fullerenol

treatment solution, were washed with PBS and directly taken for AFM indentation measurements in the RPMI-1640 media.

2.4 Cell viability assay

SMCC-7721 cells were seeded in 96-well plates at a density of 5.0×10^3 cells/well with 200 µl of RPMI-1640 media supplemented with 10% fetal bovine serum for 24 h at 37ºC in a humidified incubator with 5% of CO_2, and then exposed to the fullerenol treatment solution for 24 h, 48 h and 72 h. A 20 µl of filter sterilised MTT solution (0.5 mg/mL in PBS) was added to each well, and incubated for 4 h. After that, the blue formazan crystals trapped in cells dissolved in sterile DMSO (150 µl/well). Absorbance measurements were performed at 570 nm by a microplate reader.

2.5 Confocal imaging of actin filaments

SMCC-7721 cells were seeded in 24-well plates at a density of 2.5×10^4 cells/well and incubated for 24 h at 37ºC. After incubation, 1 ml fullerenol treatment solution was added to each well at 37ºC in a humidified incubator with 5% of CO_2 for 24 h, 48 h and 72 h, respectively. The cells without treated by the fullerenol were used as the control cells. For the staining of actin filaments, control cells and treated cells were fixed with 1 ml 4% methanol-free formaldehyde in PBS (pH 7.4) for 20 min, washed with PBS three times, and permeabilized with 1 ml 1% Triton X-100 in PBS for 4 min. A cell fluorescence imaging kit was used for labeling the actin network. A 500 µl/well of iFluor 488-phalloidin working solution was added into the fixed cells, and the cells were stained at room temperature for 1 h in a dark room. The confocal images were acquired with the Zeiss LSM 700 confocal microscope.

2.6 AFM indentation system

A commercial AFM (JPK NanoWizard® 3 BioScience) was used for cell imaging and probing the elastic modulus of living SMCC-7721 cells, and mounted on an inverted optical microscope, allowing the AFM and optical microscope imaging simultaneously. The measurements were made by a silicon nitride cantilever with the spring constant of 0.03 N/m, half-opening angle of 25 degrees, tip radius of 10 nm and height of about 2.5-8 μm. The spring constant of the cantilever was calibrated, and in the following experiments a square pyramidal tip with the spring constant of 0.027 N/m was used. The AFM tip was moved towards the sample with a 3D scanner of 100 μm in the x, y axes and 15 μm in the z axis. The image size was 512×512 pixels. SMCC-7721 cells in the physiological medium were imaged in the contact mode with a scan rate of 0.4 Hz and indented at the room temperature.

2.7 Elastic modulus measurements

The force-displacement curves were obtained from the indentation of the living cells. Fig. 1a shows a schematic of the AFM probe manipulation of living cells in the physiological medium. In the setup, the sample stage was fixed, and the AFM probe was moved by the piezoelectric scanner in the z direction towards the sample stage to implement the scanning and indentation functions. In the indentation, the AFM tip was used as an indenter and the indenting force was applied on the flexible cantilever as shown in Fig. 1b.

The indentation of the living cells can be expressed by the Hooke's law

$$F = k \cdot \delta \qquad (1)$$

where F is the indenting force on the AFM cantilever, k is the cantilever spring constant, and δ is the cantilever deflection. The displacement of the AFM tip Z is

$$Z = h + \delta \qquad (2)$$

where δ is the cantilever deflection and h is the indentation depth of sample.

The indentation response can be affected by the mechanical behavior of living cells while the geometrical shape of the AFM tip defines the contact area (Sirghi et al., 2008; Rico et al., 2007). Hertz theory (Hertz, 1881) has provided solutions about elastic indentation of half-space samples by non-deformable spherical and conical indenters. Recently, Rico et al. (2005) have developed a four-sided pyramidal model to estimate the mechanical properties of living cells with the AFM tip made of silicon or silicon nitride as shown in Fig. 1c. The shape of the AFM tip can be generally modeled as axis symmetrical geometries such as cylindrical, conical, paraboloidal, spherical and pyramidal shapes. An ideal regular square pyramidal silicon nitride AFM tip model can be expressed as (Rico et al., 2005)

$$F = \frac{1}{\sqrt{2}} \cdot \frac{E}{1-\nu^2} \cdot \tan\alpha \cdot h^2 \qquad (3)$$

where ν is the Poisson's ratio of the samples, $\nu = 0.5$ for incompressible materials which is often considered for living cells (Kirmizis et al., 2010; Mathur et al., 2001), and α is the pyramidal angle. The force F is related to the Young's modulus of the sample E and the indentation depth h. In this case, the effective radius of the contact r_c is

$$r_c = \frac{\tan\alpha}{\sqrt{2}} \cdot h \qquad (4)$$

Equation (4) shows that the effective radius of the contact r_c is a function of the pyramidal angle α and the indentation depth h. It defines the relationship among the three parameters and they can be determined according to application requirements.

3. Results and discussions

In the experiment, the contact mode AFM was used for topography imaging and mechanical nanoindentation of the cells. The biomechanical properties of SMCC-7721 cells and the cells exposed to the fullerenol ($C_{60}(OH)_{24}$) for 24 h, 48 h and 72 h respectively were investigated. With the help of an inverted optical microscope, it enabled the quick localization and selection of the target cells. The optical morphology imaging and AFM 3D imaging of the cells were implemented simultaneously, providing with the information about the cell states and biomechanical variations of the measured cells.

The effects of the fullerenol in a time series of AFM deflection and the corresponding optical morphology images of living SMCC-7721 cells are shown in Fig. 2. Depending on the fullerenol treatment periods, the morphological differences of treated cells were observed in different phases of the treatment. For the control cells (Fig. 2a), which were not exposed to the fullerenol and after cultured for 24 h in the physiological solution, the lamellipodium was fully developed, and the majority of cell shapes were polygonal. When cells were exposed to the fullerenol for 24 h (Fig. 2b), a striking morphological change of living cells from the polygon to shuttle shape and a significant increase in the average height were observed (5.06 ± 0.96 μm for control cells and 6.68 ± 2.12 μm for cells treated for 24 h, $p < 0.05$). After the treatment with the fullerenol for 48 h (Fig. 2c), the lamepllipodia was retracted and the cell shape appeared rounded, and the average height (9.01 ± 1.30 μm for 48 h, $p < 0.05$) of the cells increased significantly with the increase of the treatment period. Till the treatment period was up to 72 h (Fig. 2d), the majority of cell shapes were changed from the polygon into round, and there was a small variation in the average height (8.71 ± 1.21 μm) compared to the cells treated for 48 h. The tendency of increasing became inconspicuous. By comparison with the surface roughness of the control cells (1.26 ± 0.27 μm),

there were no obvious changes in the average surface roughness of the cells exposed to the fullerenol (1.01±0.28 μm for 24 h, 1.27±0.60 μm for 48 h and 1.2822±0.3980 μm for 72 h). The statistical analyses of the average height and surface roughness distributions of the control cells and the fullerenol treated cells are shown in Fig. 2e.

In this study, SMCC-7721 cells after treated with the fullerenol, the average height is increased and cell shapes are changed from the polygon into round. Meanwhile, as the treated periods increased, the retraction of the lamellipodium can be observed. The time-dependent effect of the fullerenol on cellular morphology is observed during 48 h. After that, the morphological effects of fullerenol show no distinct changes for SMCC-7721 cells. Studies suggest that the fullerenol interacting with the cytoskeleton has the potential to lead to the actin filament disruption and further interfere with the autophagy processing and mitochondrial function (Johnson-Lyles et al., 2010). The effects of various drugs on the cell's elastic properties have been investigated. It is found that the disruption of the actin filaments results in the decrease of the elasticity and indicates that the cell's mechanical stability is dramatically affected by the actin filaments (Rotsch and Radmacher, 2000; Ujihara et al., 2012). The alterations in cellular morphology could reveal valuable physical insights about changes in cytoskeleton, which is associated with biomechanical properties and dynamic cellular processes. Notably, the elasticity measurements can provide a powerful tool for the investigation of the physical changes of the cytoskeleton and represent the influence of the drugs on cancer cells effectively.

The elastic moduli of cells can be obtained by recording the force map. In the constant force mode, the AFM cantilever vertical deflections are correlated with the cellular elastic modulus distribution. In addition, the heterogeneous characteristic of cell mechanical properties is mainly affected by the membrane cytoskeletal heterogeneity. Thus, the elastic modulus values are

different in different cell regions (Kuznetsova et al., 2007; Pogoda et al., 2012; Roduit et al., 2008). Fig. 3a shows the topography image of a single control cell. The elasticity map of the selected cell body part (highlighted with the solid green line) with a matrix of 32×32 force curves is obtained from the measurements of the force versus the displacement, as shown in Fig. 3b. The slope of the force curve depends on the stiffness of the sample. The higher the slope, the stiffer the sample surface. The relative elastic modulus values are calculated in the range of 0-5500 Pa. The statistical distribution is shown in Fig. 3c. The dark region of the force map is corresponding to the low elastic modulus values. This region appears softer compared to the rest of the cell body.

To quantitatively determine the elastic moduli of SMCC-7721 cells, the ideal regular square pyramidal silicon nitride AFM tip model was used in the experiment. The elastic moduli were calculated from 100-300 force curves for control cells and the cells exposed to the fullerenol for 24 h, 48 h and 72 h. The Gaussian fitting curves and histograms that represent the time-series of elastic modulus versus the frequency counts distribution are shown in Figs. 4a-4d and summarized in Table 1. There are significant alterations in the elastic moduli between the control cells and the fullerenol treated cells. The elastic moduli of the cells exposed to the fullerenol for 24 h decrease significantly in the overall range compared with those of the control cells. As the treatment duration increases, the elastic moduli decrease further. Till the treatment is up to 72 h, the elastic moduli have no distinct variation compared to the cells treated with the fullerenol for 48 h. For a relative low range of 0-1000 Pa, the proportion of elastic modulus distributions of the cells exposed to the fullerenol for 24 h is increased from 42.75% to 72.11% compared with the control cells, and when the treatment time is up to 48 h, there are 95.97% elastic moduli of cells in this range. Meanwhile, the proportions of the elastic modulus distributions between 1000-2000, 2000-4000 and 3000-4000 Pa are all decreased correspondingly. Notably, when the cells are exposed to

the fullerenol up to 48 h, the elastic moduli fall below 4000 Pa. Remarkably, the effect of fullerenol on elastic modulus of the cells is found to be similar for the treatment periods of 48 h and 72 h. Although the elastic moduli fall below 3000 Pa with the treatment periods of 72 h, there are 95.78% elastic moduli of cells in the range of 0-1000 Pa, the variation of elastic modulus is not significant between the treatment periods of 48 h and 72 h. Statistical analyses suggest that, at the 0.001 level, the average elastic moduli are significantly different between the control cells (1358±501 Pa) and the cells treated with the fullerenol for 24 h (641±248 Pa). At the same level, the difference between the cells exposed to the fullerenol for 24 h and 48 h (384±117 Pa) is also significant. There is no significant difference between the treatment periods of 48 h and 72 h (404.45±242.56 pa). Fig. 4e shows the histograms of time-series of the average elastic modulus distribution.

In order to better estimate the effect of the fullerenol on SMCC-7721 cells, the control cells and the fullerenol treated cells were cultured for the same time-series, 24 h, 48 h and 72 h. The corresponding cell viability was assessed by MTT assay. Fig. 5 shows that the SMCC-7721 cells exposed to the fullerenol for 24 h have reduced cell viability to 83% ± 3.31%. After treated for 48 h, cell viability has reduced to 66% ± 4.19%. Meanwhile, the control cells have increased the viability to 165.1% ± 2.15%, compared with the control cells cultured for 24 h. The cells exposed to the fullerenol for 72 h have reduced viability to 52.84% ± 3.72%, whereas the untreated cells have increased the cell viability to 182.4% ± 2.343%.The average elastic moduli of the cells exposed to the fullerenol for 24 h and 48 h show a diminishing trend compared with those control cells, which is associated with the alteration of the cellular cytoskeleton network stiffness. Furthermore, the indentation force and depth of penetrating into the cell membrane are significantly different between the control cells and the cells treated with the fullerenol under the

same condition of the AFM mechanical parameters used. The force-indentation curves of the control cells and the cells exposed to the fullerenol are shown in Fig. 6a. The relationships of the stiffnesses between the control cells and the exposed cells are clearly shown by the force-indentation curves. After the cells exposed to the fullerenol, the stiffnesses significantly decrease. Meanwhile, it can be seen that the forces of penetrating into the cell membranes decrease as well in this case. When the AFM tip contacts the control cell surface, it continues to indent and the force increases till point 1 (P1) in the indentation process, hereafter a sudden force relaxation is observed instead of increasing continuously. Then the force suffers a period of fluctuation, and after that the force increases rapidly, which could be caused by the AFM tip contacting the substrate. The force relaxed point that can be regarded as the position in which the AFM tip has penetrated into the cell membrane successfully (Han et al. 2005). The penetration points of the cells treated with the fullerenol for 24 h, 48 h and 72 h are shown at points 2 (P2), 3 (P3) and 4 (P4), respectively. Statistical analyses suggest that the declining trends of the average penetration depth and force distribution are obtained with the increase of the treatment duration, which is similar to the elastic modulus distribution. With exposed to the fullerenol for 24 h, the average penetration depth (0.66 ± 0.28 μm, $p < 0.001$) and force (0.33 ± 0.08 nN, $p < 0.001$) are significantly decreased compared with the control cells (1.40 ± 0.40 μm and 0.64 ± 0.29 nN). Keeping a constant concentration, the average penetration depth (0.41 ± 0.28 μm, $p < 0.05$) and force (0.22 ± 0.09 nN, $p < 0.01$) of the cells treated with the fullerenol for 48 h are significantly less than those treated with the fullerenol for 24 h. Till treated for 72 h (0.4317 ± 0.15 μm and 0.27 ± 0.09 nN), there are no significant variations in the values of average penetration depth and force compared to the cell treatment for 48 h. Fig. 6b shows the average penetration depth and

average penetration force of the control cells and the cells exposed to the fullerenol for 24 h, 48 h and 72 h, and the measurements are performed for 10, 16, 14 and 13 cells, respectively.

The measurements of the effects of the fullerenol on the mechanics of living SMCC-7721 cells indicate that the cell stiffness is decreased with the increase of the fullerenol treatment periods. It is known that the actin network plays a key role in the cellular mechanical stability. The disruption of the actin network causes a dynamic reduction of cell stiffness. The confocal image of the control cells represents that numerous long bundles of actin filaments are observed obviously, and the majority of cell shapes are polygonal (Fig. 7a). When cells are exposed to the fullerenol for 24 h, the bundles of actin filaments are transformed into actin aggregates and distributed irregularly within the cells (Rubtsova et al., 1998). Moreover, the conversion of actin filaments from long bundles to punctate structures is revealed (Fig. 7b). After the treatment with the fullerenol for 48 h, the numbers of long actin filaments are reduced significantly. Most of the cells are retracted and the cell shapes appeare rounded (Fig. 7c). Till the treatment period up to 72 h, almost all the long actin filament bundles are collapsed and hairy structures are observed, as shown in Fig. 7d. The experiment demonstrates that the changes of the cellular morphology and actin cytoskeleton treatment with the fullerenol show a partial similarity with the effects of cytoskeleton disruption indueced by Cytochalasin D as a common reagent to perturb the actin cytoskeleton consequently and affect the mechanical properties of cells (Hayot et al, 2006; Rubtsova et al., 1998; Shoji et al., 2012).

4. Conclusion

The correlation of AFM data and optical morphology images was obtained to better understand the effect of the fullerenol on living SMCC-7721 cells. The dynamic processes of the fullerenol

induced changes in cellular morphology were recorded in the optical morphology and AFM images. In this work, the fullerenol $C_{60}(OH)_{24}$ induced changes of elasticity in living SMCC-7721 cells have been studied by AFM indentation. Quantitative measurements of biomechanical properties during the fullerenol treatment were performed by recording time-series of elastic moduli, penetration forces and penetration depths on the cells. A gradual decrease in the biomechanical parameters of living SMCC-7721 cells as a consequence of the fullerenol treatment could be caused by the disruption of actin filaments. Till the cells treated for 72 h, the average elastic modulus is reduced by a factor of approximately 3.4. The values for the average indentation force and depth of penetrating into the cell membrane are decreased 2.4-folds and 3.3-folds, respectively. Additionally, the dynamic cellular changes are accompanied with morphology changes. For a given concentration of the fullerenol, the cell shapes changed from the polygon into round have been observed as the result of the time dependent effect. The decrease in the average elastic modulus could be caused by the fullerenol cytotoxicity induced actin filaments disruption, which plays an important role in the cell's mechanical stability. Therefore, the observations presented in this paper can also be instructive to improve the understanding of the alterations of biomechanical properties of SMCC-7721 cells affected by the fullerenol, and the potential for an anticancer drug based on fullerenol applications.

Acknowledgment

This work was supported by International Science and Technology Cooperation Program of China (No.2012DFA11070), Special Development Program of Central Financial Support to Local Universities (No.2011-183), EU FP7 (ECNANOMAN No.269219; ECROBOT No.318971; BioRA No.612641), Jilin Provincial Science and Technology Program (No.20100703, No.201024 and No.201215136), and Science and Technology Program of Changchun City (No.10GH15 and No.11KP04).

References

Aryaei, A., Jayasuriya, A.C., 2013. Mechanical properties of human amniotic fluid stem cells using nanoindentation. Journal of Biomechanics. 46, 1524-1530.

Binnig, G., Quate, C.F., Gerber, C.h., 1986. Atomic force microscope. Physical Review Letters. 56, 930-933.

Bosi, S., Ros, T.D., Spalluto, G., Prato, M., 2003. Fullerene derivatives: an attractive tool for biological applications. European Journal of Medicinal Chemistry. 38, 913-923.

Chen, Z., Ma, L., Liu, Y., Chen, C., 2012. Applications of functionalized fullerenes in tumor theranostics. Theranostics. 2, 238-250.

Chen, Z., Mao, R., Liu, Y., 2012. Fullerenes for cancer diagnosis and therapy: Preparation, Biological and Clinical Perspectives. Current Drug Metabolism. 13, 1035-1045.

Cross, S.E., Jin, Y.S., Rao, J., Gimzewski, J.K., 2007. Nanomechanical analysis of cells from cancer patients. Nature Nanotechnology. 2, 780-783.

Desjardins, L.M., MacManus, J.P., 1995. An adherent cell model to study different stages of apoptosis. Experimental Cell Research. 216, 380-387.

Dong, C., Kashon, M.L., Lowry, D., Dordick, J.S., Reynolds, S.H., Rojanasakul, Y., Sargent, L.M., Dinu, C.Z., 2013. Exposure to carbon nanotubes leads to changes in the cellular biomechanics. Advanced Healthcare Materials. 2, 945-951.

Etienne-Manneville, S., 2004. Actin and microtubules in cell motility: which one is in control. Traffic. 5, 470-477.

Foleya, S., Bosib, S., Larroquec, C., Pratob, M., Janota, J., Setaa, P., 2001. Photophysical properties of novel water soluble fullerene derivatives. Chemical Physics Letters. 350, 198-205.

Fuchs, E., Karakesisoglou, I., 2001. Bridging cytoskeletal intersections. Genes & Development. 15, 1-14.

Fuhrmann, A., Staunton, J.R., Nandakumar, V., Banyai, N., Davies, P.C., Ros, R., 2011. AFM stiffness nanotomography of normal, metaplastic and dysplastic human esophageal cells. Physical Biology. 8, 015007.

GLOBOCAN 2012: Estimated Cancer Incidence, Mortality, and Prevalence Worldwide in 2012, World Health Organization. http://globocan.iarc.fr/Default.aspx.

Han, S.W., Nakamura, C., Obataya, I., Nakamura, N., Miyake, J., 2005. A molecular delivery system by using AFM and nanoneedle. Biosensors and Bioelectronics. 20, 2120-2125.

Hayot, C., Debeir, O., Ham, P.V., Damme, M.V., Kiss, R., Decaestecker, C., 2006. Characterization of the activities of actin-affecting drugs on tumor cell migration. Toxicology and applied pharmacology. 211, 30-40.

Hertz, H., 1881. On the elastic contact of elastic solids. Journal für die reine und angewandte Mathematik. 92, 156-171.

Imajoh, M., Sugiura, H., Oshima, S.I., 2004. Morphological changes contribute to apoptotic cell death and are affected by caspase-3 and caspase-6 inhibitors during red sea bream iridovirus permissive replication.Virology. 322, 220-230.

Jensen, A.W., Wilson, S.R., Schuster, D.I., 1996. Biological applications of fullerenes. Bioorganic & Medicinal Chemistry. 4, 767-779.

Johnson-Lyles, D.N., Peifley, K., Lockett, S., Neun, B.W., Hansen, M., Clogston, J., Stern, S.T., McNeil, S.E., 2010. Fullerenol cytotoxicity in kidney cells is associated with cytoskeleton disruption, autophagic vacuole accumulation, and mitochondrial dysfunction. Toxicology and Applied Pharmacology. 248, 249-258.

Jonietz, E., 2012. Mechanics: The forces of cancer. Nature. 491, S56–S57.

Kirmizis, D., Logothetidis, S., 2010. Atomic force microscopy probing in the measurement of cell mechanics. International Journal of Nanomedicine. 5, 137-145.

Kojić, V., Jakimov, D., Bogdanović, G., Đorđević, A., 2005. Effects of fullerenol $C_{60}(OH)_{24}$ on cytotoxicity induced by antitumor drugs on human breast carcinoma cell lines. Materials Science Forum. 494, 543-548.

Kumar, S., Weaver, V.M., 2009. Mechanics, malignancy, and metastasis: The force journey of a tumor cell. Cancer and Metastasis Reviews. 28, 113-127.

Kuznetsova, T.G., Starodubtseva, M.N., Yegorenkov, N.I., Chizhik, S.A., Zhdanov, R.I., 2007. Atomic force microscopy probing of cell elasticity. Micron. 38, 824-833.

Lautenschläger, F., Paschke, S., Schinkinger, S., Bruel, A., Beil, M., Guck, J., 2009. The regulatory role of cell mechanics for migration of differentiating myeloid cells. In Proceedings of the National Academy of Sciences. University of Cambridge, Cambridge.

Lee, G.Y., Lim, C.T., 2007. Biomechanics approaches to studying human diseases. Trends in Biotechnology. 25, 111-118.

Lekka, M., Laidler, P., Gil, D., Lekki, J., Stachura, Z., Hrynkiewicz, A.Z., 1999. Elasticity of normal and cancerous human bladder cells studied by scanning force microscopy. European Biophysics Journal. 28, 312-316.

Li, Q.S., Lee, G.Y., Ong, C.N., Lim, C.T., 2008. AFM indentation study of breast cancer cells. Biochemical and Biophysical Research Communications. 374, 609-613.

Lu, L.H., Lee, Y.T., Chen, H.W., Chiang, L.Y., Huang, H.C., 1998. The possible mechanisms of the antiproliferative effect of fullerenol, polyhydroxylated C_{60}, on vascular smooth muscle cells. British Journal of Pharmacology. 123, 1097-1102.

Maciaszek, J.L., Lykotrafitis, G., 2011. Sickle cell trait human erythrocytes are significantly stiffer than normal. Journal of Biomechanics. 44, 657-661.

Mason, B.N., Califano, J.P., Reinhart-King, C.A., 2012. Matrix stiffness: a regulator of cellular behavior and tissue formation. In: Bhatia, S.K. (Eds.), Engineering Biomaterials for Regenerative Medicine. Springer, New York, pp. 19-37.

Mathur, A.B., Collinsworth, A.M., Reichert, W.M., Kraus, W.E., Truskey, G.A., 2001. Endothelial, cardiac muscle and skeletal muscle exhibit different viscous and elastic properties as determined by atomic force microscopy. Journal of Biomechanics. 34, 1545–1553.

Mrdanović, J., Solajić, S., Bogdanović, V., Stankov, K., Bogdanović, G., Djordjevic, A., 2009. Effects of fullerenol $C_{60}(OH)_{24}$ on the frequency of micronuclei and chromosome aberrations in CHO-K1 cells. Mutation Research/Genetic Toxicology and Environmental Mutagenesis. 680, 25-30.

Nielsen, G.D., Roursgaard, M., Jensen, K.A., Poulsen, S.S., Larsen, S.T., 2008. In vivo biology and toxicology of fullerenes and their derivatives. Basic & Clinical Pharmacology & Toxicology. 103, 197-208.

Nikolaev, N.I., Müller, T., Williams, D. J., Liu, Y., 2014. Changes in the stiffness of human mesenchymal stem cells with the progress of cell death as measured by atomic force microscopy. Journal of Biomechanics. 47, 625-630.

Ujihara, Y., Nakamura, M., Miyazaki, H., Wada, S., 2012. Contribution of actin filaments to the global compressive properties of fibroblasts. Journal of the Mechanical Behavior of Biomedical Materials. 14, 192-198.

Unterberger, M.J., Schmoller, K.M., Bausch, A.R., Holzapfel, G.A., 2013. A new approach to model cross-linked actin networks: multi-scale continuum formulation and computational analysis. Journal of the Mechanical Behavior of Biomedical Materials. 22, 95-114.

Partha, R., Conyers, J.L., 2009. Biomedical applications of functionalized fullerene-based nanomaterials. International Journal of Nanomedicine. 4, 261-275.

Plodinec, M., Loparic, M., Monnier, C.A., Obermann, E.C., Zanetti-Dallenbach, R., Oertle, P., Hyotyla, J.T., Aebi, U., Bentires-Alj, M., Lim, M.R., Schoenenberger, C.A., 2012. The nanomechanical signature of breast cancer. Nature Nanotechnology. 7, 757-765.

Pogoda, K., Jaczewska, J., Wiltowska-Zuber, J., Klymenko, O., Zuber, K., Fornal, M., Lekka, M., 2012. Depth-sensing analysis of cytoskeleton organization based on AFM data. European Biophysics Journal. 41, 79-87.

Rade, I., Natasa, R., Biljana, G., Aleksandar, D., Borut, S., 2008. Bioapplication and activity of fullerenol $C_{60}(OH)_{24}$. African Journal of Biotechnology. 27, 4940-4050.

Rico, F., Roca-Cusachs, P., Gavara, N., Farré, R., Rotger, M., Navajas, D., 2005. Probing mechanical properties of living cells by atomic force microscopy with blunted pyramidal cantilever tips. Physical Review E. 72, 021914 (1)-(10).

Rico, F., Roca-Cusachs, P., Sunyer, R., Farré, R., Navajas, D., 2007. Cell dynamic adhesion and elastic properties probed with cylindrical atomic force microscopy cantilever tips. Journal of Molecular Recognition. 20, 459-466.Roduit, C., van der Goot, F.G., De Los Rios, P., Yersin, A., Steiner, P., Dietler, G., Catsicas, S., Lafont, F., Kasas, S., 2008. Elastic membrane heterogeneity of living cells revealed by stiff nanoscale membrane domains. Biophysical Journal. 94, 1521-1532.

Rotsch, C., Braet, F., Wisse, E., Radmacher, M., 1997. AFM imaging and elasticity measurements on living rat liver macrophages. Cell Biology International. 21, 685-696.

Rotsch, C., Radmacher, M., 2000. Drug-induced changes of cytoskeletal structure and mechanics in fibroblasts: an atomic force microscopy study. Biophysical Journal. 78, 520-535.

Rubtsova, S.N., Kondratov, R.V., Kopnin, P.B., Chumakov, P.M., Kopnin, B.P., Vasiliev, J.M., 1998. Disruption of actin microfilaments by cytochalasin D leads to activation of p53. FEBS Letters. 430, 353-357.Saraste, A., Pulkki, K., 2000. Morphologic and biochemical hallmarks of apoptosis. Cardiovascular Research. 45, 528-537.

Sayes, C.M., Fortner, J.D., Guo, W., Lyon, D., Boyd, A.M., Ausman, K.D., Tao, Y.J., Sitharaman, B., Wilson, L.J,, Hughes, J.B., West, J.L., Colvin, V.L., 2004. The differential cytotoxicity of water-soluble fullerenes. Nano Letters. 4, 1881-1887.

Shimizu, K., Kubota, R., Kobayashi, N., Tahara, M., Sugimoto, N., Nishimura, T., Ikarashi, Y., 2013. Cytotoxic effects of hydroxylated fullerenes in three types of liver cells. Materials. 6, 2713-2722.

Shoji, K., Ohashi, K., Sampei, K., Oikawa, M., Mizuno, K., 2012. Cytochalasin D acts as an inhibitor of the actin–cofilin interaction Biochemical and biophysical research communications. 424, 52-57.

Sirghi, L., Ponti, J., Broggi, F., F. Rossi., 2008. Probing elasticity and adhesion of live cells by atomic force microscopy indentation. Eur. Biophys. J. 37, 935-945.

Tian, F., Cui, D., Schwarz, H., Estrada, G.G., Kobayashi, H., 2006. Cytotoxicity of single-wall carbon nanotubes on human fibroblasts. Toxicol In Vitro. 20, 1202–1212.

Walker, V.G., Li, Z., Hulderman, T., Schwegler-Berry, D., Kashon, M.L., Simeonova, P.P., 2009. Potential in vitro effects of carbon nanotubes on human aortic endothelial cells. Toxicol Appl Pharmacol. 236, 319–328.

Xu, W., Mezencev, R., Kim, B., Wang, L., McDonald, J., Sulchek, T., 2012. Cell stiffness is a biomarker of the metastatic potential of ovarian cancer cells. PLoS One. 7, e46609 (1)-(12).

Yoo, L., Reed, J., Shin, A., Demer, J.L., 2014. Atomic force microscopy determination of Young's modulus of bovine extra-ocular tendon fiber bundles. Journal of Biomechanics. In press. http://dx.doi.org/10.1016/j.jbiomech.2014.02.011

Zhou, Y.T., Guy, G.R., Low, B.C., 2006. BNIP-Sa induces cell rounding and apoptosis by displacing p50RhoGAP and facilitating RhoA activation via its unique motifs in the BNIP-2 and Cdc42GAP homology domain. Oncogene. 25, 2393-2408.

Zhu, Y., Dong, Z., Wejinya, U.C., Jin, S., Ye, K., 2011. Determination of mechanical properties of soft tissue scaffolds by atomic force microscopy nanoindentation. Journal of Biomechanics. 44, 2356-2361.

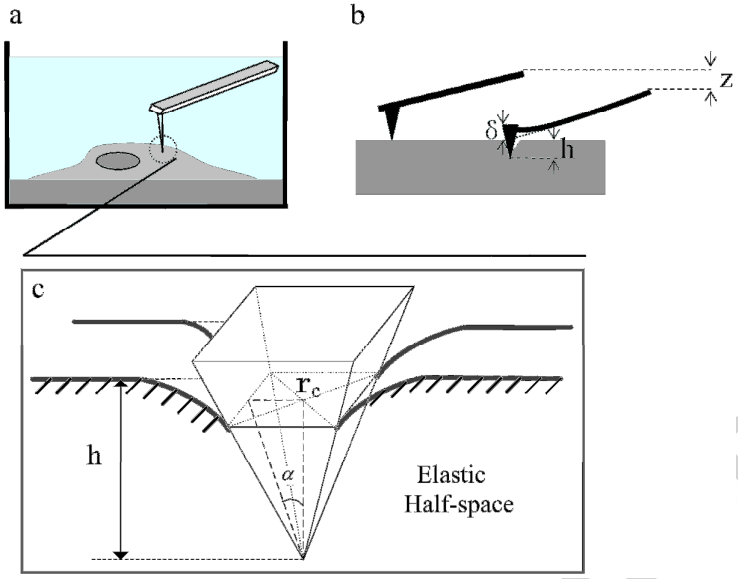

Fig. 1 a A single living cell imaged and indented by an AFM probe in the physiological medium. **b** The principle of an AFM tip used as an indenter showing the relationship between the vertical displacement of the AFM tip *Z*, cantilever deflection δ and indentation depth of sample h ($Z = h+\delta$). **c** A schematic of the indentation of an elastic half-space sample using a square pyramidal silicon nitride AFM tip where α is the pyramidal angle and r_c is the indenter-sample contact radius.

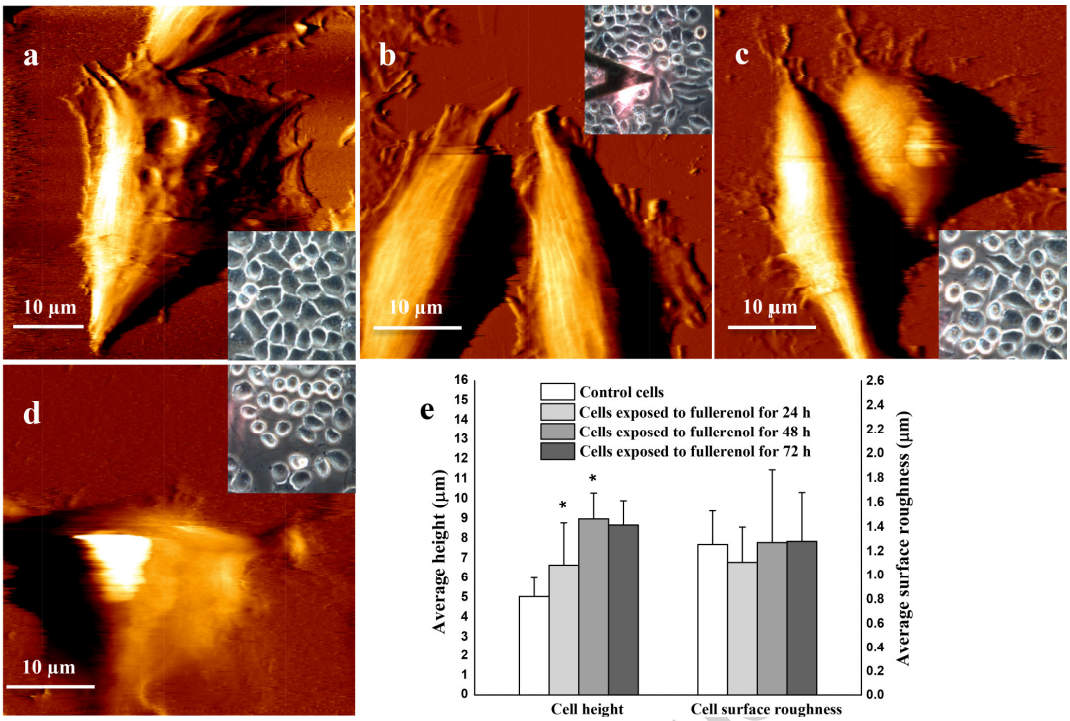

Fig. 2 Time series of optical morphology and AFM deflection imaging of the living SMCC-7721 cells: **a** A control cell surface image in the physiological medium with the scanning range of 50 μm × 50 μm. **b**, **c, d** Surface images of SMCC-7721 cells exposed to the fullerenol for 24 h, 48 h and 72 h with the scanning range of 40 μm × 40 μm. **e** Statistical analyses of the average height and surface roughness distribution of control cells and the cells exposed to the fullerenol for 24 h, 48 h and 72 h. The increasing of the average height between the control cells vs the cells exposed to the fullerenol for 24 h and the cells exposed to the fullerenol for 24 h vs 48 h are significant. The differences were considered statistically significant at *$p < 0.05$. The optical morphology images were acquired at 20× magnification, and the cellular morphologies changed from the polygon into round, as shown in Figs. 2a to 2d.

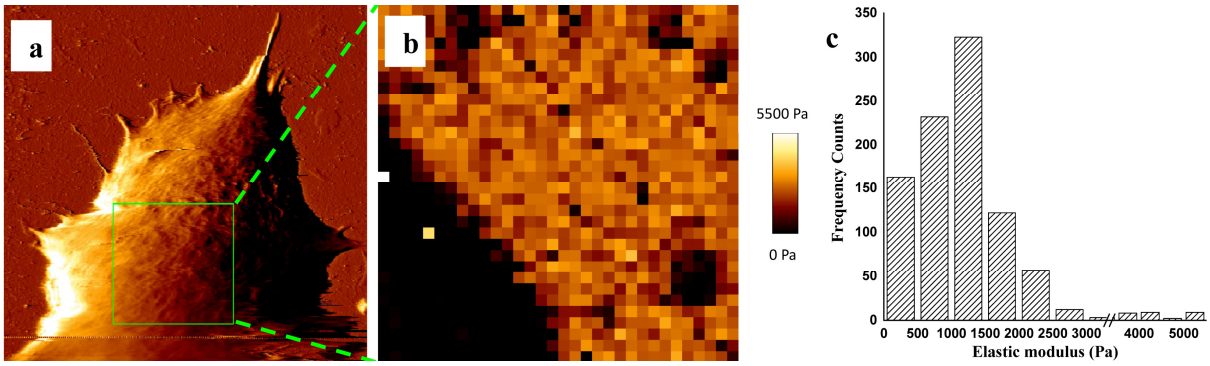

Fig. 3 a Deflection image of single control cells with the scanning range of 45 µm×45 µm. **b** The elasticiy map with a matrix of 32×32 force curves of the selected cell body part. The scanning range is 14.5 µm×14.5µm and highlighted with the solid green line. **c** Statistical distribution of the elastic modulus; The relative elastic moduli values are calculated in the range of 0-5500 Pa.

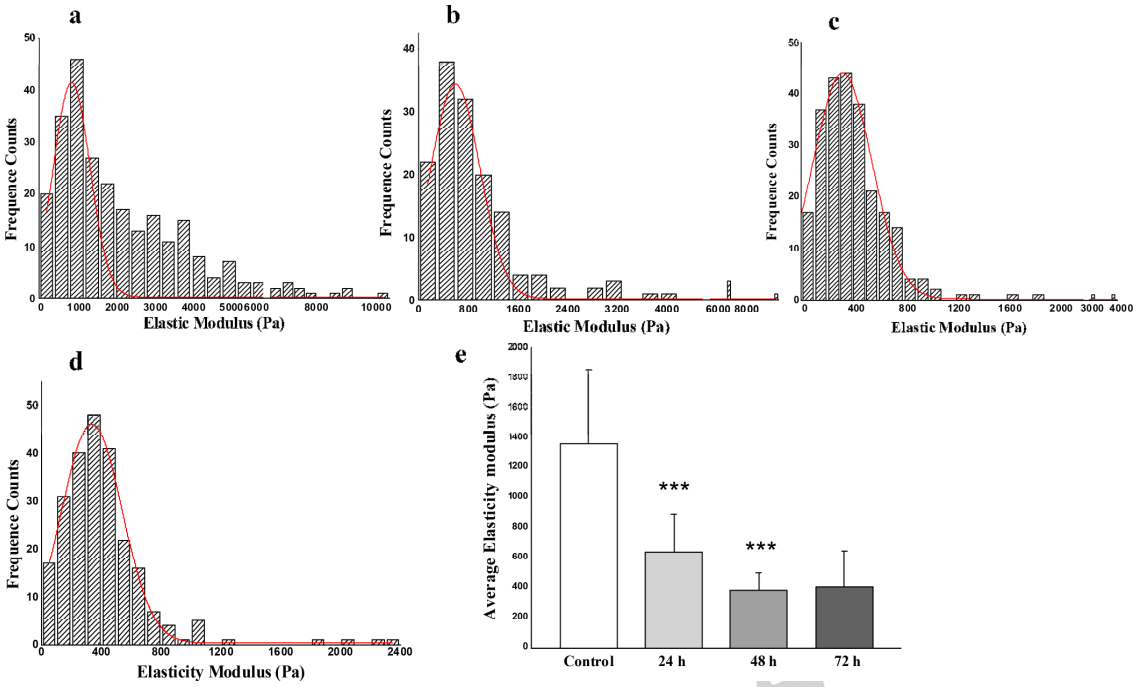

Fig. 4 Histograms showing the time-series of elastic modulus-frequency count distribution of living SMCC-7721 cells during treatment with the fullerenol, and the Gaussian fit curves. The control cells as a reference before treatment of the fullerenol (**a**) and the cells exposed to the fullerenol for 24 h (**b**), 48 h (**c**) and 72 h (**d**) respectively. **e** Statistical analyses of the time-series of average elastic moduli. The differences between the control cells vs the cells exposed to the fullerenol for 24 h and the cells exposed to the fullerenol for 24 h vs 48 h are significant. The differences are considered statistically significant at ***$p < 0.001$. After 72 h, no distinct effects on elasticity.

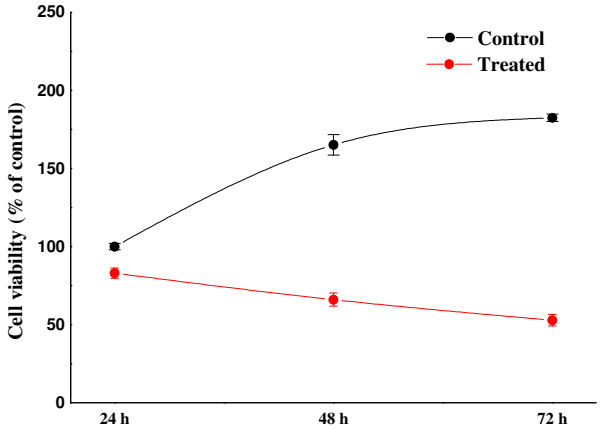

Fig. 5 SMCC-7721 cell viability assays. The control cells and the fullerenol treated cells were cultured for the same time-series of 24 h, 48 h and 72 h, respectively. Cell viability was determined at each time point by the MTT assay. Values correspond to the mean ± standard error, N=3.

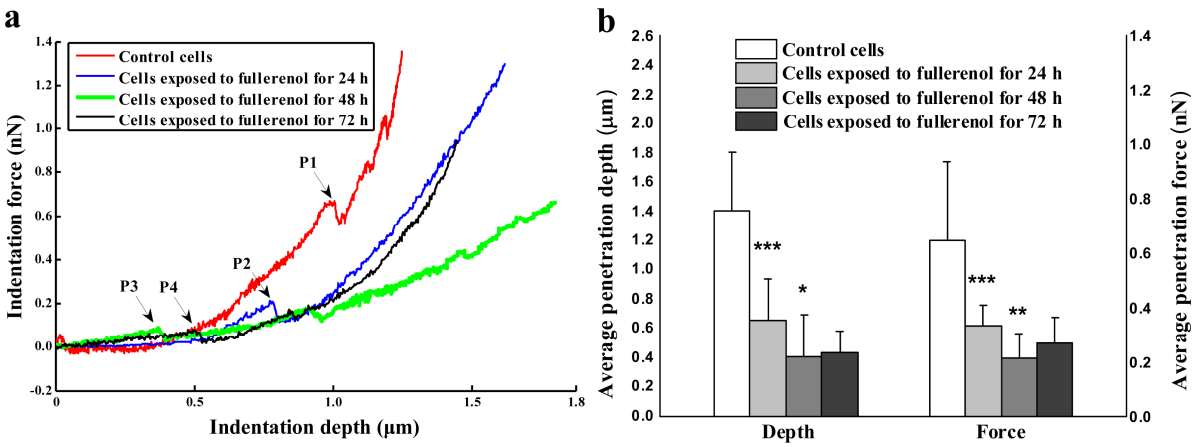

Fig. 6 a Force-indentation curves of the control cells and the cells exposed to the fullerenol. P1, P2, P3 and P4 are the penetration points of the control cells and the cells treated with the fullerenol for 24 h, 48 h and 72 h, respectively. **b** Statistical analyses of average penetration depths and forces of the control cells and cells treated with the fullerenol for 24 h 48 h and 72 h. The differences of average penetration depths and forces are significant between the control cells vs the cells treated with the fullerenol for 24 h (***$p < 0.001$ for depths and forces) and the cells treated with the fullerenol for 24 h and 48 h (*$p < 0.05$ for depths and **$p < 0.01$ for forces).

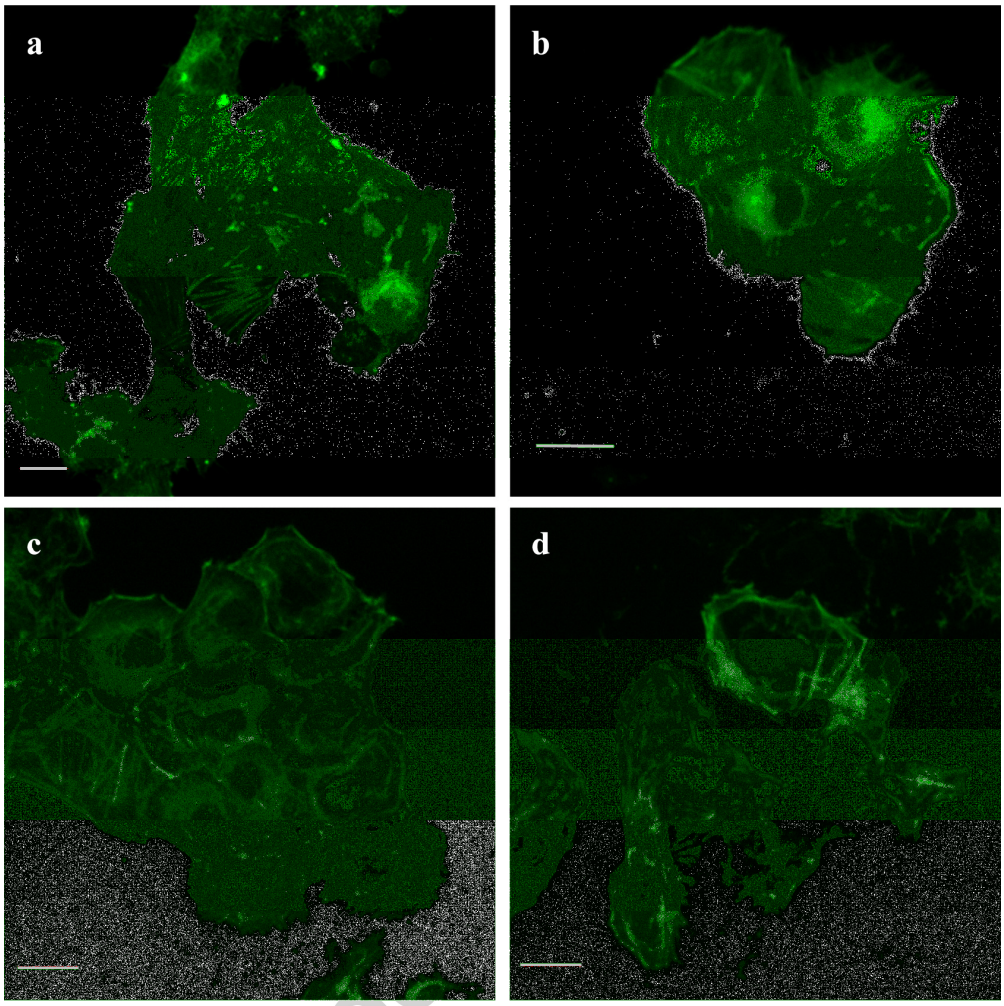

Fig. 7 Confocal images show the effect of fullerenol ($C_{60}(OH)_{24}$) on actin filaments in SMCC-7721 cells. **a** Actin filaments staining in control cells. **b**, **c** and **d** are the cell treated by the fullerenol for 24 h, 48 h and 72 h, respectively. Images taken with ×20 objective. (Scale bar: 20 μm).

Table 1 Time series of elastic modulus distributions of the living SMCC-7721 cells treated with fullerenol.

Group	Counts	0-1000 Pa	1000-2000 Pa	2000-3000 Pa	3000-4000 Pa	>4000 Pa
Control cells	262	42.75%	20.99%	14.12%	9.92%	12.22%
Cells incubated with fullerenol for 24 h	148	72.11%	18.37%	3.40%	2.72%	3.40%
Cells incubated with fullerenol for 48 h	249	95.97%	2.41%	0.81%	0.81%	0%
Cells incubated with fullerenol for 72 h	237	95.78%	2.95%	1.27%	0%	0%